



Soft Matter

**Activated Penetrant Dynamics in Glass Forming Liquids:
Size Effects, Decoupling, Slaving, Collective Elasticity and
Correlation with Matrix Compressibility**

Journal:	<i>Soft Matter</i>
Manuscript ID	SM-ART-12-2020-002215.R1
Article Type:	Paper
Date Submitted by the Author:	17-Jan-2021
Complete List of Authors:	Mei, Baicheng; University of Illinois at Urbana-Champaign, Schweizer, Kenneth; University of Illinois at Urbana-Champaign,

SCHOLARONE™
Manuscripts

**Activated Penetrant Dynamics in Glass Forming Liquids: Size Effects, Decoupling,
Slaving, Collective Elasticity and Correlation with Matrix Compressibility**

Baicheng Mei^{ad} and Kenneth S. Schweizer^{*abcd}

a. Department of Materials Science, University of Illinois, Urbana, IL 61801, USA

b. Department of Chemistry, University of Illinois, Urbana, IL 61801, USA

c. Department of Chemical & Biomolecular Engineering, University of Illinois, Urbana, IL 61801, USA

d. Materials Research Laboratory, University of Illinois, Urbana, IL 61801, USA

*kschweiz@illinois.edu

Abstract

We employ the microscopic self-consistent cooperative hopping theory of penetrant activated dynamics in glass forming viscous liquids and colloidal suspensions to address new questions over a wide range of high matrix packing fractions and penetrant-to-matrix particle size ratios. The focus is on the mean activated relaxation time of smaller tracers in a hard sphere fluid of larger particle matrices. This quantity also determines the penetrant diffusion constant and connects directly with the structural relaxation time probed in an incoherent dynamic structure factor measurement. The timescale of the non-activated fast dissipative process is also studied and is predicted to follow power laws with the contact value of the penetrant-matrix pair correlation function and the penetrant-matrix size ratio. For long time penetrant relaxation, in the

relatively lower packing fraction metastable regime the local cage barriers are dominant and matrix collective elasticity effects unimportant. As packing fraction and/or penetrant size grows, much higher barriers emerge and the collective elasticity associated with the correlated matrix dynamic displacement that facilitates penetrant hopping becomes important. This results in a non-monotonic variation with packing fraction of the degree of decoupling between the matrix and penetrant alpha relaxation times. The conditions required for penetrant hopping to become slaved to the matrix alpha process are determined, which depend mainly on the penetrant to matrix particle size ratio. By analyzing the absolute and relative importance of the cage and elastic barriers we establish a mechanistic understanding of the origin of the predicted exponential growth of the penetrant hopping time with size ratio predicted at very high packing fractions. A dynamics-thermodynamics power law connection between the penetrant activation barrier and the matrix dimensionless compressibility is established as a prediction of theory, with different scaling exponents depending on whether matrix collective elasticity effects are important. Quantitative comparisons with simulations of the penetrant relaxation time, diffusion constant, and transient localization length of tracers in dense colloidal suspensions and cold viscous liquids reveal good agreements. Multiple new predictions are made that are testable via future experiments and simulations. Extension of the theoretical approach to more complex systems of high experimental interest (nonspherical molecules, semiflexible polymers, crosslinked networks) interacting via variable hard or soft repulsions and/or short range attractions is possible, including under external deformation.

I. Introduction

Understanding the dynamics and transport of dilute “penetrants” or “tracers” in atomic, molecular, and polymer liquids and glasses, and the nanoparticle or colloidal suspension analogues, is a fundamental scientific problem of broad interest¹⁻⁸. Relevant applications for the former systems include gas and organic molecule separations in rubbery, supercooled melt and vitrified polymer membranes where large selectivity and rapid transport are desired⁵⁻⁸, barrier materials that suppress gas permeation in coatings^{9, 10}, self-healing applications based on controlled release of reactive molecules from microcapsules^{9, 10}, and ion and solvent transport in biological and polymeric materials^{7, 11}. Existing models are almost entirely phenomenological, typically built around the difficult to quantify idea of “free volume”^{7, 8, 11-13}. Even for simple sphere models, how penetrant transport depends on its size relative to that of the matrix particles, over a wide range of temperature and density where the matrix alpha relaxation process can vary up to 14 decades, is not well established, with different models making qualitatively different predictions^{11, 14}. For example, the logarithm of the long time penetrant diffusion constant has been argued to vary linearly, quadratically, and as the third power of penetrant size^{15, 16}. A variety of simulations^{14,17-23} using different models have been performed. Most recently, a comprehensive study¹⁴ of atomic and molecular penetrants in dense polymeric media found that for spherical tracers the diffusion constant scales as the exponential of one power of the penetrant diameter. However, more broadly, the study of penetrant transport is computationally challenging since it is often activated and hence quite slow, which can restrict such studies to situations where penetrant diffusivity is sufficiently high. This renders the construction of predictive theories of particularly high value.

Tracer nanoparticle or colloid diffusion in a dense suspension or glass composed of larger particles is also of major interest²⁴⁻³⁰. Since colloids are typically 100-1000 times larger than molecules (e.g., 100 nm to 1 μm vs 1 nm), *equilibrium* transport and relaxation is measurable over far fewer decades (6-9 less). The matrix kinetically vitrifies when a tracer activation barrier is far less than those of thermal liquids, a limitation that also applies to simulations. Since equilibrium states with very high activation barriers for transport are not probed, ideal mode coupling theory (MCT)³¹ can provide insight. However, its lack of activated processes can incur qualitative errors for the *long time* matrix alpha relaxation process in the colloidal domain, and even more so for viscous liquids.

From a theoretical perspective, we believe the key to making progress for both colloidal and molecular systems is to have a predictive theory of pure matrix activated dynamics, and how it is coupled with, or facilitates, activated penetrant hopping. Recently, Zhang and Schweizer³² formulated such an approach at a microscopic force level in the dilute penetrant limit: the self-consistent cooperative hopping (SCCH) theory, which builds on the Elastically Collective Nonlinear Langevin Equation (ECNLE) theory^{33, 34} of the pure matrix alpha relaxation process. SCCH theory addresses in a mechanistic manner how matrix activated motion and emergent shear rigidity determine the penetrant hopping rate. The latter is a central issue in the separation membranes community^{7, 8} where permeability involves the product of the penetrant solubility and diffusion constant (scales as the hopping rate), with the latter typically more strongly varying with molecular size, shape, and thermodynamic state¹⁴. The physical ideas of SCCH theory bear some similarity with classic problems in solid state physics, e.g., small polaron transport³⁵ and interstitial diffusion in crystals³⁶, where local steric obstruction and correlated collective elasticity of the medium (phonons) play crucial roles.

Although formulated at the stochastic trajectory level^{37, 38} from which one can, in principle, determine time-dependent correlation functions^{39, 40}, SCCH theory has focused on a subset of key average dynamical quantities, most importantly the penetrant structural or alpha relaxation time. Knowledge of the latter allows a direct estimate of the penetrant diffusion constant (inverse proportionality)^{32, 41, 42} and is connected to measurements of the mean time scale for the decay of the wavevector (q) dependent penetrant incoherent dynamic structure factor on the local cage (q^*) scale, $F_s(q=q^*, t)$.

Specific numerical applications of SCCH theory to date have been for the simplest model: a hard sphere penetrant dissolved in a dense hard sphere fluid or glass³². This model is directly relevant to atomic penetrants in atomic liquids (e.g., rare gases)^{43, 44} and spherical nanoparticles in colloidal suspensions^{3, 45}. Based on a mapping of chemical complexity to an effective hard sphere mixture model, it can also be applied to molecular penetrants in molecular and polymeric matrices^{32, 41, 42}. By varying the penetrant size and attractive interactions with the matrix, penetrant diffusion was studied at the level of model calculations and (via the mapping) confronted with experiments. For example, successful predictions were made based on one adjustable parameter for the diffusivity as a function of temperature of water, toluene, methanol, and oxygen in polyvinylacetate liquids and glasses³². At the underlying hard sphere model level, the logarithm of the penetrant diffusion constant was predicted to be *linearly* related to the size asymmetry ratio over a specific thermodynamic-state-dependent parameter range³², which appears to be qualitatively consistent with simulations^{14, 21, 22, 46}, especially the very recent study of ref.14. Moreover, to leading order this size ratio dependence appears to be weakly dependent on penetrant-matrix attraction^{14, 32}, emphasizing the importance of steric effects due to repulsive forces for this question. SCCH theory has also been tentatively extended to treat penetrant

dynamics in athermal (no attractions) two-component spherical particle mixtures⁴², with a successful application to understand the concentration dependence of toluene diffusivity in toluene-polystyrene mixtures.

However, the prior theoretical work in the dilute penetrant limit³² was highly limited with the following issues not addressed. (i) The nature and relevance of the short time/length scale dissipative penetrant relaxation process. (ii) The evolution of the activated penetrant relaxation (hopping) time or diffusivity over the entire metastable fluid range that can be probed in experiment and simulation. (iii) The detailed physical origin and range of validity of the nearly exponential connection between the penetrant relaxation time (inverse diffusion constant) and size ratio. (iv) Do connections exist for penetrant relaxation or diffusivity with easily measurable thermodynamic properties of the matrix? The primary goal of the present article is to address these scientific questions.

In addition, a generic technical issue is that all prior SCCT work^{32, 41, 42} adopted integral equation theory (IET) with the Percus-Yevick (PY) closure⁴⁷ to compute the structural correlations required to quantify dynamical constraints. Very recently we explored the consequences for dynamically-relevant thermodynamic properties and structure in glass forming liquids by using the modified-Verlet (MV) closure approximation. By quantitatively confronting the more thermodynamically-consistent MV based results and their PY closure analogues with simulations in the dense metastable fluid regime we demonstrated the former predicts much more accurate structural correlations and thermodynamics in one-component fluids⁴⁸ and two-component mixtures⁴⁹ than its PY-based analogue. Since the foundational idea of the ECNLE and SCCH theories is a direct connection between activated dynamics and structure, the accuracy of structural input can significantly impact some dynamical predictions and conclusions drawn

from their confrontation with experiment and simulation. As a recent example of this issue we found that by using the improved MV closure structural information in ECNLE theory a novel linear correlation between a thermodynamic property and activated relaxation time in one-component hard sphere fluids is predicted⁵⁰. Hence, improved structural input to the dynamical theory is especially important for addressing issue (iv) above.

In this article we study the above issues using SCCH theory and accurate IET input for the foundational model of a dilute hard sphere penetrant in a dense hard sphere matrix fluid. Section II reviews the theoretical background and model employed. Section III presents new results for activated penetrant relaxation and its decoupling from, or slaving to, the matrix alpha relaxation, the nature and role of the short time/distance non-activated penetrant relaxation process, and the mechanism of exponential size dependence of penetrant relaxation time. How the key results of section III are correlated with thermodynamics and a metric of short time/distance dynamics is studied in section IV. Section V summarizes our most important testable predictions and compares some of them against simulations of molecular and colloidal tracer diffusion. The article concludes in section VI with a summary and a discussion of opportunities for future generalizations of both the model and theory to treat more complex systems. A few additional technical results and figures are collected in the Supplementary Information (SI).

II. Background and Theory

All the required theoretical methods for this study have been described previously³². Thus, we only sketch below without derivation the results germane to our present work, beginning with ECNLE theory³³ and SCCH theory³² in sub-sections IIA and IIB, respectively, and then the

equilibrium structural input in sub-section IIC. The reader interested only in our new results can proceed directly to section III. However, Figures 1 and 2 below contain important background results for all our subsequent dynamical analyses and physical discussions.

A. ECNLE theory for one-component fluids

The ECNLE theory³³ for one-component fluids directly enters SCCH theory³² since in the dilute penetrant limit the matrix dynamics is taken to be unperturbed. The starting point is a NLE for the stochastic trajectory of a tagged (spherical) particle in the overdamped limit^{37,38}:

$$-\xi_s \frac{dr(t)}{dt} - \frac{\partial}{\partial r} F_{\text{dyn}}(r(t)) + \delta\eta(t) = 0 \quad (1)$$

Here, $r(t)$ denotes the scalar particle displacement at time t from its initial position, the friction coefficient ξ_s quantifies the short time/distance relaxation process, $F_{\text{dyn}}(r)$ is the displacement-dependent “dynamic free energy” containing contributions from all slowly relaxing components of the forces exerted on a tagged particle by its surroundings, and $\delta\eta$ is the white noise random force that satisfies $\langle \delta\eta(t)\delta\eta(0) \rangle = 2\beta^{-1}\xi_s\delta(t)$, where $\beta = 1/k_B T$ is the inverse thermal energy with k_B Boltzmann’s constant and T temperature. The dynamic free energy, $F_{\text{dyn}}(r)$, is^{37,38}:

$$\beta F_{\text{dyn}}(r) = -3\ln(r/\sigma) - \int \frac{d\mathbf{q}}{(2\pi)^3} \frac{\rho C^2(q)S(q)}{1+S^{-1}(q)} e^{\left[-q^2 r^2 (1+S^{-1}(q))/6\right]} \quad (2)$$

The second term corresponds to a trapping potential that favors dynamic localization. It is quantified by ρ (fluid number density) and the pair structure in Fourier space ($S(q)$, the structure factor) which is related to the direct correlation function as $C(q) = \rho^{-1}[1 - S^{-1}(q)]$. In the absence of noise, or if the dynamic free energy is approximated by a harmonic form, eqn (1) reduces to the single particle naïve mode coupling theory (NMCT) self-consistent equation³⁸ for the long-time limit of the particle mean square displacement or localization length which obeys:

$$r_{\text{loc}}^{-2} = \frac{1}{9} \int \frac{d\mathbf{q}}{(2\pi)^3} q^2 \rho C^2(q) S(q) e^{(-q^2 r_{\text{loc}}^2/6)[1+1/S(q)]} \quad (3)$$

For hard spheres, a kinetic transition is predicted at $\phi \sim 0.43$, beyond which a transiently localized state and barrier emerge in the dynamic free energy signaling a crossover to activated motion³⁷.

Whether the system is below or above the dynamic crossover, the elementary time scale is set by $\xi_s = k_B T / D_s = k_B T \tau_s / \sigma^2$, where σ is the particle diameter, D_s the short time diffusion constant, and τ_s the fast process relaxation time. The non-activated short time relaxation process includes binary collisions and non-self-consistent caging effects^{37, 51-53}. In the “normal fluid” regime before the NMCT crossover is reached, it corresponds to the structural alpha relaxation time. This regime is experimentally relevant for colloidal suspensions, but typically not for supercooled viscous liquids under isobaric conditions over the accessible range of temperatures. In the activated regime, this timescale controls short distance motion before many body caging and transient localization emerge; it also enters as an attempt time scale for barrier hopping. In either case, for a Newtonian hard sphere fluid one has^{33, 50}:

$$\begin{aligned} \tau_s &= \tau_E \left[1 + \frac{\rho}{6\pi^2} \int_0^\infty dq \frac{q^2 C^2(q) S(q)}{1 + n(q)/S(q)} \right] \\ \tau_E &= \tau_0 g(\sigma), \quad \tau_0 = 16\phi\sigma \sqrt{\beta M / \pi} \end{aligned} \quad (4)$$

where M is particle mass, $g(\sigma)$ the contact value of the pair correlation function, and $1/n(q) = 1 - j_0(q) + 2j_2(q)$ with $j_\alpha(q)$ the Bessel function of order α . In practice, we find replacing $1/n(q)$ with unity has *negligible* influence on τ_s .

All our computed relaxation times are expressed in terms of the elementary time scale, τ_0 . For atomic or molecular viscous liquids a characteristic value is $\tau_0 \sim 1$ ps. In contrast, for colloidal suspensions τ_0 is determined by the dilute Stokes-Einstein problem, with τ_0 scaling as

particle diameter cubed. Hence, in a colloidal suspension of spheres of diameter ~ 100 nm to 1 μm , τ_0 is ~ 6 -9 decades longer than that for a viscous liquid. This difference has large consequences on the magnitude of the activation barrier at the laboratory (or computer) glass transition.

An example dynamic free energy computed using the MV closure for structural input is shown in the inset of Fig. 1. The dynamic free energy has a minimum at r_{loc} (transient dynamic localization length), a maximum at the barrier location, r_{B} , and a local cage barrier, F_{B} . With increasing packing fraction, r_{B} and F_{B} grow but r_{loc} decreases, resulting in a microscopic jump distance $\Delta r \equiv r_{\text{B}} - r_{\text{loc}}$ that increases with packing fraction. Calculations^{37, 50} based on structural input using the PY or MV closure predict to a good approximation $\beta F_{\text{B}} \propto \sigma/r_{\text{loc}}$, which also scales linearly with the inverse dimensionless compressibility $1/S(q=0) = S_0^{-1}$. The latter is a thermodynamic property that quantifies the amplitude of long wavelength density fluctuations.

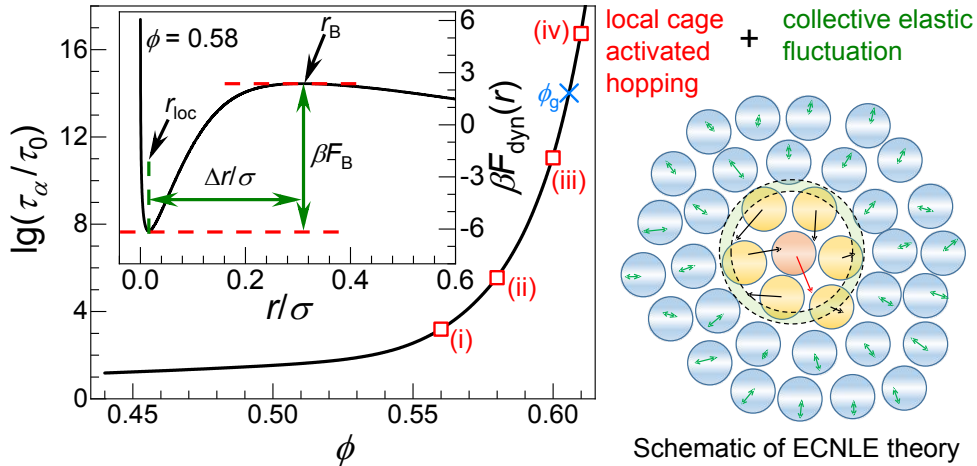


Fig. 1 Main: structural alpha relaxation time (in units of τ_0) predicted by ECNLE theory for one-component hard sphere fluids as a function of packing fraction ϕ based on OZ-MV structural input⁴⁸. The kinetic glass transition (indicated as the blue cross at $\phi \sim 0.605$) is defined as when $\tau_\alpha/\tau_0 = 10^{14}$ which corresponds to 100 seconds in a viscous liquid with $\tau_0 \sim \text{ps}$. Other specific packing fractions we study in detail for the penetrant problem are indicated as red squares. For

viscous liquids (elementary object size ~ 1 nm) these correspond to: (i) a lower packing fraction state where cooperative elasticity just begins to be important ($\phi = 0.56$, $\tau_\alpha \sim 1.6$ ns, $F_{el}/F_B \sim 0.27$, $\beta F_{el} \sim 1.57$), (ii) an intermediate packing fraction state ($\phi = 0.58$, $\tau_\alpha \sim 359$ ns, $F_{el}/F_B \sim 0.53$, $\beta F_{el} \sim 4.45$), (iii) a very high packing fraction state ($\phi = 0.60$, $\tau_\alpha \sim 0.25$ s, $F_{el}/F_B \sim 1.11$, $\beta F_{el} \sim 13.46$), and (iv) slightly beyond the kinetic glass transition ($\phi = 0.61$, $\tau_\alpha \sim 10^5$ s, $F_{el}/F_B \sim 1.68$, $\beta F_{el} \sim 24.25$). For a suspension of $1 \mu\text{m}$ (100 nm) colloids, τ_0 is typically 9 (6) decades longer, and hence kinetic arrest is predicted to occur at roughly $\phi_g \sim 0.58$ (0.59) corresponding to a significantly lower activation barrier. Inset: Dynamic free energy (units of thermal energy) versus scaled particle displacement computed using OZ-MV structural input at $\phi = 0.58$; relevant length and energy scales are indicated. The right panel sketches the physical ideas of ECNLE theory³³.

Since activated relaxation involves a relatively large amplitude displacement ($\Delta r \approx 0.25\sigma \sim 0.4\sigma$), it has been argued that a small amount of extra space (cage expansion) is required to allow such a barrier hopping motion, a physical picture motivated by the phenomenological elastic ‘‘shoving model’’ of Dyre⁵⁴⁻⁵⁶. Including this physics in the NLE theory framework defines ECNLE theory³³, and introduces longer-range collective elastic fluctuation of particles outside the cage that becomes important at sufficiently low temperature/high density. The elastic displacement field outside the cage of radius r_{cage} (defined from the first minimum of the pair correlation function, $g(r)$) is given by^{33, 55}:

$$u(r) \equiv \Delta r_{\text{eff}} \left(r_{\text{cage}}/r \right)^2, \quad r \geq r_{\text{cage}} \quad (5a)$$

where the cage expansion amplitude is of order, or smaller than, r_{loc} , and is:

$$\Delta r_{\text{eff}} \equiv \frac{\int_{r_{\text{cage}} - \Delta r/4}^{r_{\text{cage}}} dr [r - (r_{\text{cage}} - \Delta r/4)] r^2}{\int_0^{r_{\text{cage}}} dr r^2} = \frac{3}{r_{\text{cage}}^3} \left[\frac{r_{\text{cage}}^2 \Delta r^2}{32} - \frac{r_{\text{cage}} \Delta r^3}{192} + \frac{\Delta r^4}{3072} \right] \approx \frac{3\Delta r^2}{32r_{\text{cage}}} \quad (5b)$$

The corresponding elastic dynamic free energy cost at a distance r from the cage center is $K_0 u^2(r)/2$, where K_0 is the harmonic curvature of $F_{\text{dyn}}(r)$ at r_{loc} . Its total contribution to the activation barrier follows by summing the contributions from all particles outside the cage³³:

$$\beta F_{\text{el}} = 4\pi \int_{r_{\text{cage}}}^{\infty} dr r^2 \rho g(r) u^2(r) K_0 / 2 \approx 2\pi \rho r_{\text{cage}}^3 \Delta r_{\text{eff}}^2 K_0 \quad (6)$$

The final result assumes $g(r)=1$, a benign simplification for hard-spheres. Based on eqn (6), and given the limited change of ρ and r_{cage} in the strongly metastable regime where collective elasticity is important, one finds the elastic barrier is determined mainly by two factors: the 4th power of the particle jump distance, Δr^4 , and the localized state spring constant, K_0 . The latter is related to the dynamic (relaxed) shear modulus as $G' \sim \phi K_0$,^{33, 38, 57} which is quantitatively more important in a *relative* sense than the jump distance contribution^{33, 48} to the elastic barrier.

The alpha relaxation event is then a coupled local-nonlocal process involving coordinated cage scale hopping and a longer range elastic fluctuation, with the total barrier equal to the sum of the local cage and collective elastic contributions. The alpha time follows as $\tau_\alpha = \tau_s + \tau_{\text{hop}}$, where the mean first passage or barrier hopping time is computed using Kramers theory^{58, 59} as:

$$\begin{aligned} \tau_{\text{hop}} &= \frac{2\tau_s e^{\beta F_{\text{el}}}}{\sigma^2} \int_{r_{\text{loc}}}^{r_{\text{loc}}+\Delta r} dr e^{\beta F_{\text{dyn}}(r)} \int_{r_{\text{loc}}}^r dr' e^{-\beta F_{\text{dyn}}(r')} \\ &\approx \tau_s \frac{2\pi}{\sqrt{K_0 K_B}} e^{\beta(F_B + F_{\text{el}})} \end{aligned} \quad (7)$$

The second expression is accurate beyond a local cage barrier of order 1-2 thermal energy units. We note in passing that based on OZ-MV structural input we find the factor $\tau_s/\sqrt{K_0 K_B}$ is essentially *independent* of packing fraction and equals $\sim 0.13\tau_0$ (units of K_j are set to unity). Hence, the hopping time is controlled by the exponential of the total barrier in thermal energy units. This finding is relevant in our analysis below in that conclusions drawn from analyzing the logarithm of the alpha time or total activation barrier are effectively identical.

The main frame of Fig. 1 presents calculations of the alpha time as a function of packing fraction. Collective elastic physics is unimportant when $\phi = 0.44-0.56$, followed by a crossover at $\phi = 0.56$ where $\beta F_{\text{el}} \sim 1.5$, beyond which elasticity effects increasingly dominate for $\phi = 0.56-$

0.60 leading to many decades of increase of the relaxation time, and ultimately kinetic vitrification at $\phi \sim 0.605$. The latter is deduced from the criterion that $\tau_\alpha/\tau_0 = 10^{14}$, corresponding to 100 s for a thermal liquid with $\tau_0 = 1$ ps. In the very slow activated regime, we recently showed⁵⁰ that the logarithm of alpha time scales as the 3rd power of the inverse dimensionless compressibility, versus as the 1st power when the local cage barrier dominates.

B. SCCH theory in the dilute penetrant limit

In the dilute penetrant (diameter d) limit, the analogue of eqn (1) for the instantaneous penetrant displacement (trajectory) from its initial position, r_p , is^{32, 42}

$$-\zeta_{s,p} \frac{dr_p}{dt} - \frac{\partial}{\partial r} F_{\text{dyn,p}} + \delta\eta_p = 0 \quad (8)$$

where $\delta\eta_p$ is the white noise random force corresponding to the short time friction constant

$\zeta_{s,p} = k_B T \tau_{s,p} / d^2$ associated with penetrant-matrix interactions (here collisions). Repeating the

NMCT analysis yields the self-consistent equation for the penetrant localization length^{32, 42}

$$r_{\text{loc,p}}^{-2} = \frac{N_p}{9} \int \frac{d\mathbf{q}}{(2\pi)^3} q^2 \rho C_{\text{mp}}^2(q) \omega_p(q) S_{\text{mm}}(q) e^{(-q^2 r_{\text{loc,p}}^2 / 6)} e^{[-q^2 r_{\text{loc,m}}^2 / 6 S_{\text{mm}}(q)]} \quad (9)$$

Information about the pure matrix static structure factor, penetrant-matrix pair correlation function, and the matrix dynamic localization length all enter eqn (9).

Based on eqn (9), the penetrant dynamic free energy obeys^{32, 42}:

$$\frac{\partial \beta F_{\text{dyn,p}}(r_p, r_m)}{\partial r_p} = -\frac{3}{r_p} + \frac{r_p}{3} \int \frac{d\mathbf{q}}{(2\pi)^3} q^2 \rho C_{\text{mp}}^2(q) S_{\text{mm}}(q) e^{(-q^2 r_p^2 / 6)} e^{[-q^2 r_m^2 / 6 S_{\text{mm}}(q)]} \quad (10)$$

which depends on *both* dynamic displacement variables, r_p and r_m , reflecting the coupling of penetrant motion to matrix displacements *at* the trajectory level. This complicated aspect is approximately handled in SCCH theory (see Fig. 2) by introducing the idea of a cooperative

displacement variable via a single ‘‘coupling’’ parameter, γ . The latter quantifies the magnitude of slow (matrix) and fast (penetrant) displacements in the coupled motion as^{32, 42}:

$$r_m(\gamma) = r_{loc,m} + (r_p - r_{loc,p})/\gamma \quad (11)$$

Substituting eqn (11) into eqn (10), the penetrant dynamic free energy follows via numerical integration of eqn (10).

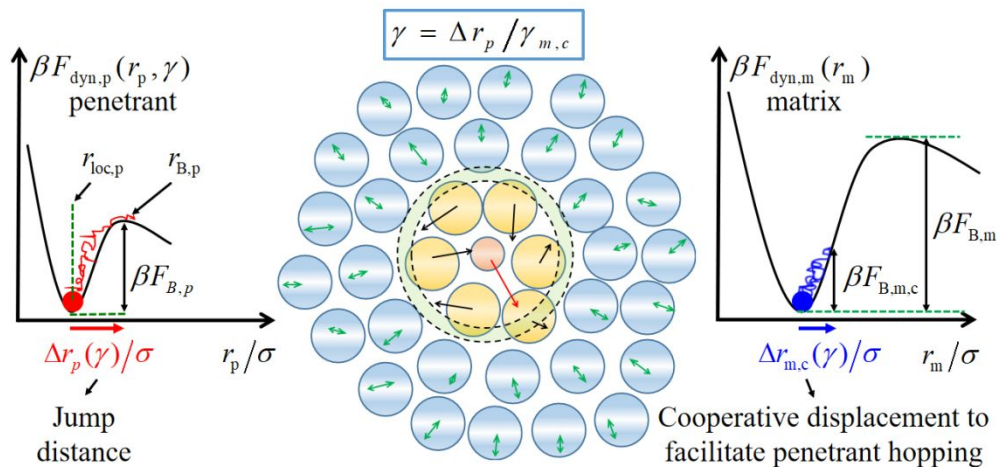


Fig. 2 Key ingredients of the two coupled dynamic free energies in SCCH theory of a single spherical penetrant in a bulk matrix of larger diameter spheres. Matrix facilitation of penetrant hopping is formulated based on the concept of a dimensionless dynamic coupling parameter, γ , defined as the ratio of the penetrant particle jump distance $\Delta r_p(\gamma)$ to the matrix particle facilitating displacement, $\Delta r_{m,c}(\gamma)$. Relevant length and energy scales are indicated. The middle schematic displays the physical ideas of SCCH theory for the penetrant problem.

The coupling parameter γ is predicted by enforcing a temporal self-consistency condition.

The penetrant jump distance corresponding to $F_{dyn,p}(r_p, \gamma)$ is denoted as $\Delta r_p(\gamma) = r_{B,p}(\gamma) - r_{loc,p}$, and the corresponding correlated displacement of the matrix particles is $\Delta r_{m,c}(\gamma) = \Delta r_p(\gamma)/\gamma$.

The temporal self-consistency condition follows as^{32, 42}:

$$\tau_{hop,p}[\Delta r_p(\gamma)] = \tau_{dis,m}[\Delta r_{m,c}(\gamma)] \quad (12)$$

The mean penetrant hopping time is again computed using Kramers theory,

$$\tau_{\text{hop,p}}(\gamma) = \frac{2\tau_{\text{s,p}} e^{\beta F_{\text{el,p}}(\gamma)}}{d^2} \int_{r_{\text{loc,p}}}^{r_{\text{loc,p}} + \Delta r_{\text{p}}(\gamma)} dr_{\text{p}} e^{\beta F_{\text{dyn,p}}(r_{\text{p}},\gamma)} \int_{r_{\text{loc,p}}}^{r_{\text{p}}} dr'_{\text{p}} e^{-\beta F_{\text{dyn,p}}(r'_{\text{p}},\gamma)}, \quad (13)$$

where $\tau_{\text{s,p}} = d^2/D_{\text{s,p}}$ is the characteristic penetrant short-time scale, given as^{32, 42}:

$$\tau_{\text{s,p}} = \tau_{\text{E,p}} \left[1 + \frac{\rho}{6\pi^2} \int_0^\infty dq \frac{q^2 C_{\text{mp}}^2(q) S_{\text{mm}}(q)}{1 + (\sigma^2 \tau_{\text{E,p}}/d^2 \tau_{\text{E,m}}) n(q)/S_{\text{mm}}(q)} \right] \quad (14)$$

$$\tau_{\text{E,p}} = d^2/D_{\text{E,p}} = \tau_0 \frac{d^2 d_{\text{mp}}^2}{\sigma^4} \left(\frac{2m}{M+m} \right)^{1/2} g_{\text{mp}}(d_{\text{mp}})$$

Here, $d_{\text{mp}} = (d + \sigma)/2$, m is penetrant mass with $m/(m + M) = d^3/(d^3 + \sigma^3)$, $g_{\text{mp}}(d_{\text{mp}})$ is the contact value of $g_{\text{mp}}(r)$, and the penetrant alpha time is $\tau_{\alpha,\text{p}} = \tau_{\text{s,p}} + \tau_{\text{hop,p}}$. The mean time required for a matrix particle to self-consistently displace a distance $\Delta r_{\text{m,c}}(\gamma)$ is denoted as $\tau_{\text{dis,m}}[\Delta r_{\text{m,c}}(\gamma)]$.

It is computed using the Kramers mean first passage time equation,

$$\tau_{\text{dis,m}}(\Delta r_{\text{m,c}}(\gamma)) = \frac{2\tau_{\text{s,m}} e^{\beta F_{\text{el,m,c}}(\gamma)}}{\sigma^2} \int_{r_{\text{loc,m}}}^{r_{\text{loc,m}} + \Delta r_{\text{m,c}}(\gamma)} dr_{\text{m}} e^{\beta F_{\text{dyn,m}}(r_{\text{m}})} \int_{r_{\text{loc,m}}}^{r_{\text{m}}} dr'_{\text{m}} e^{-\beta F_{\text{dyn,m}}(r'_{\text{m}})} \quad (15)$$

$$\approx \tau_{\text{s,m}} \frac{2\pi}{\sqrt{K_{0,\text{m}} K_{\text{B,m}}}} e^{\beta(F_{\text{B,m,c}} + F_{\text{el,m,c}})}$$

Equations (13) and (15) include the elastic barrier contribution in a way that acknowledges that the motion of the penetrant to its barrier and the facilitating matrix displacement is a *single* time correlated dynamical event, and hence the elastic cost obeys^{32, 42} $F_{\text{el,p}} = F_{\text{el,m,c}}$.

The collective elastic barrier accompanying the penetrant hop is constructed following the same basic method discussed above. In the dilute limit a penetrant (matrix) hop is treated as on average requiring an outward radial motion of amplitude $\Delta r_{\text{p}}(\gamma)/4$ ($\Delta r_{\text{m,c}}(\gamma)/4$). The angularly averaged effective cage dilation amplitude follows as^{32, 42}:

$$\Delta r_{\text{eff,p}}(\gamma) = \frac{3}{r_{\text{cage,p}}^3} \left[\frac{r_{\text{cage,p}}^2 \Delta r_{\text{m,c}}^2(\gamma)}{32} - \frac{r_{\text{cage,p}} \Delta r_{\text{m,c}}^3(\gamma)}{192} + \frac{\Delta r_{\text{m,c}}^4(\gamma)}{3072} \right] \approx \frac{3}{32} \frac{\Delta r_{\text{m,c}}^2(\gamma)}{r_{\text{cage,p}}} \quad (16)$$

where $r_{\text{cage,p}} = r_{\text{min,mp}}$ with $r_{\text{min,mp}}$ the cage radius corresponding to the first minimum of $g_{\text{mp}}(r)$.

The elasticity cost for any a particle at a distance r from the cage center is then $K_{0,m} u_p^2(r)/2$,

with $u_p(r) \equiv \Delta r_{\text{eff,p}} \left(r_{\text{cage,p}}/r \right)^2$ for $r \geq r_{\text{cage,p}}$. The total elastic barrier associated with the

facilitating matrix motion follows by summing the contributions from all particles outside the penetrant cage region, and is given by^{32, 42}:

$$\beta F_{\text{el,p}} = 2\pi \int_{r_{\text{cage,p}}}^{\infty} dr r^2 \rho g_{\text{mp}}(r) u_p^2(r) K_{0,m} / 2 \approx 2\pi r_{\text{cage,p}}^3 \Delta r_{\text{eff,p}}^2 \rho K_{0,m} \quad (17)$$

where the final result again adopts $g_{\text{mp}}(r) = 1$ outside the cage. This elastic barrier is determined mainly by two contributions: the matrix dynamic fluctuation distance ($\Delta r_{\text{m,c}} = \Delta r_p / \gamma$) and matrix rigidity as encoded in $\rho K_{0,m}$. Inserting eqn (17) into eqn (13) and (15), the SCCH theory^{32, 42} is then self-consistently constructed.

C. Structural Pair Correlations

The required structural pair correlation functions are computed using the standard OZ integral equation which in Fourier space is given for the pure matrix by⁴⁷:

$$h(q) = C(q) + \rho C(q)h(q) = C(q)S(q) \quad (18)$$

Here, $h(q)$ is the Fourier transform of $h(r) = g(r) - 1$, $g(r)$ the radial distribution function, and $c(r)$ the real space direct correlation function. Based on eqn (18) plus the PY or MV closure, $g(r)$ can be numerically computed. The PY closure for hard spheres is⁴⁷ $c(r) = 0$, $r > \sigma$. For pure hard sphere fluids and mixtures the more sophisticated and accurate MV closure is^{48, 49, 60-62}:

$$b_{ij}^{\text{MV}}(r) = \frac{-a_1 \lambda_{ij}^2(r)}{1 + a_2 |\lambda_{ij}(r)|} \quad (19)$$

where $\lambda_{ij}(r) \equiv h_{ij}(r) - c_{ij}(r)$ with i and j labeling the particle type (m or p) and $a_1 = 0.5$ and $a_2 = 0.8$. The matrix-penetrant OZ equation is^{32, 47}:

$$h_{mp}(q) = C_{mp}(q)S_{mm}(q) \quad (20)$$

where the MV closure is as stated in eqn (19) and the PY closure is $c_{mp}(r) = 0$, at $r > d_{mp}$. The integral equations are numerically solved using standard methods.

Figures 3a and 3b present example calculations of the pair correlations functions for the pure matrix and penetrant-matrix analogues, respectively. The main feature of the former is the contact value grows with packing fraction, while for the latter the contact value decreases as the penetrant becomes smaller. The inset of Fig. 3a shows the matrix ‘‘cage order parameter’’ defined as the value of the first peak of $S_{mm}(q)$. It grows significantly with packing fraction reflecting the increasing coherence of local packing. The examples in these plots cover a wide range of matrix packing fractions of interest dynamically (all in the metastable regime of the hard sphere fluid), spanning the range from when the matrix barrier is nearly zero ($\phi=0.5$) to beyond ~ 32 ($\phi=0.605$) per the pure matrix kinetic glass transition discussed in section IIA.

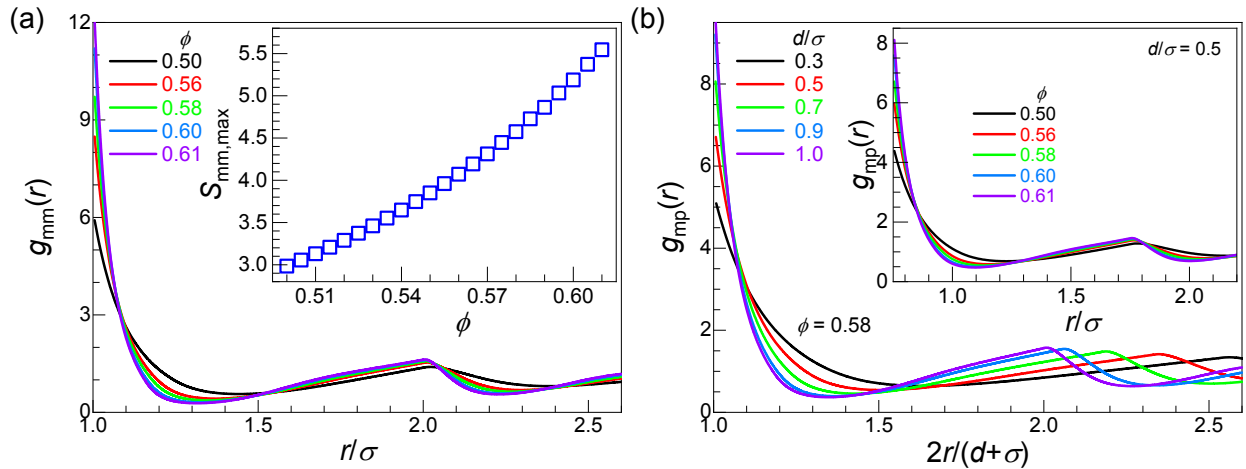


Fig. 3 (a) Main: Matrix pair correlation function as a function of scaled separation using OZ-MV theory at several packing fractions. Inset: Maximum of the matrix structure factor at its cage peak as a function of packing fraction. (b) Main: Penetrant-matrix pair correlation function using

the OZ-MV theory for several penetrant sizes as a function of scaled r at a fixed packing fraction ($\phi = 0.58$). Inset: same quantity for several packing fractions at a fixed penetrant size ($d/\sigma = 0.7$).

III. Penetrant Hopping Rate and Decoupling from the Matrix Alpha Process

Before presenting our new results we provide some background concerning how the calculations relate to simulation and experiment. Our focus is on the penetrant relaxation time associated with the short time non-activated process, $\tau_{s,p}$, and its long time alpha process analogue, $\tau_{\alpha,p}$. Both relate to two types of observables: (i) short and long time penetrant tracer diffusion constants which scale inversely with these relaxation times^{32, 41, 42}, and (ii) single particle structural relaxation times extracted, for example, from analyzing characteristic decay times of the penetrant incoherent dynamic structure factor of a “2-step” form⁶³ for wavevectors of order of the penetrant cage scale. These two time scales are analyzed over a wide range of size ratios, d/σ , and matrix packing fractions, ϕ . The latter variable is directly relevant to colloidal suspensions, and indirectly to viscous liquids via its determination of the matrix alpha time. The quantitative relation between packing fraction and the matrix alpha time is given in Figure 1. Recall that viscous (colloidal) bulk systems can be analyzed experimentally in the activated dynamics regime over ~ 14 (5-6) orders of magnitude of alpha relaxation timescale.

All the numerical results presented below employ the improved MV closure to determine structural input. They are all new with two exceptions: the main frame of Fig.6 and parts of Fig. 7 which were previously analyzed³² using the PY closure. We find quantitative, but important, differences between dynamical predictions based on MV versus PY structural inputs.

A. Short Time Non-Activated Relaxation

We first analyze the time scale of the non-activated short time process, $\tau_{s,p}$, per eqn(14). Fig. 4 presents numerical calculations of this quantity as a function of the cross constant value,

g_{mp}^{contact} , which grows monotonically with matrix packing fraction in a size ratio dependent manner (Figure 3). Interestingly, a power law relationship is predicted, $\tau_{s,p}/\tau_0 = A(g_{mp}^{\text{contact}})^{\nu}$ at each fixed d/σ , where the common exponent $\nu \sim 7/3$ over the wide range of penetrant sizes from $d = 0.3\sigma$ to $d = \sigma$ (one-component fluid). Per eqn (14), one power is due to the penetrant-matrix binary collision rate (i.e., $\tau_{E,p}$) which grows linearly with g_{mp}^{contact} . The second term in the square bracket of eqn (14) is associated with weak many body caging effects and we can deduce that it contributes to $\tau_{s,p}$ via the contact value raised to the $\sim 4/3$ power. This behavior can be precisely understood, as explained in the SI.

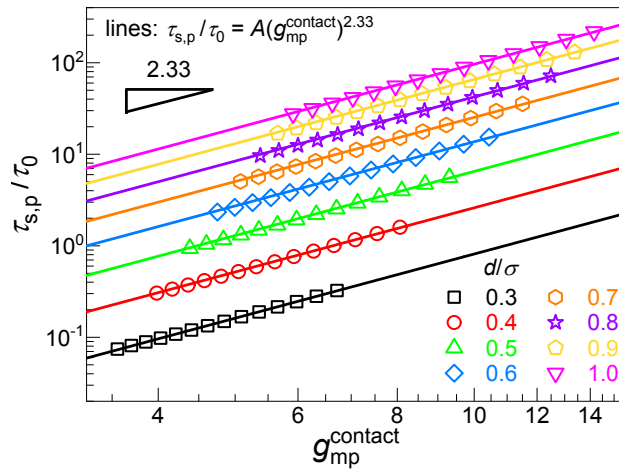


Fig. 4 Penetrant short relaxation time (units of τ_0) as a function of penetrant-matrix cross contact value over a wide range of matrix packing fractions (0.5-0.63) and size ratios, d/σ .

Despite the universal power law behavior in Fig. 4, the short time scale does increase in absolute magnitude with penetrant size even at fixed g_{mp}^{contact} . This trend arises from the prefactor

A in the relation $\tau_{s,p}/\tau_0 = A(g_{mp}^{\text{contact}})^{7/3}$. Based on numerical calculations (not shown), we find that

to a very good approximation A is proportional to the 4th power of the penetrant diameter since

from eqn (14) one has $\tau_{s,p}/\tau_0 \sim d^2 d_{mp}^2 [2m/(M+m)]^{1/2} \sim d^4$. The final scaling follows from the

denominator in the integrand of eqn (14) having a contribution that scales as $(d_{mp}/d)^2 [2m/(M+m)]^{1/2}$ which partially cancels common factors in $\tau_{s,p}/\tau_0$, leading to the d^4 scaling.

Finally, we note in passing that for one-component hard spheres the contact value is directly related to pressure, a thermodynamic property⁴⁷. Considering our recent discovery using ECNLE theory and the MV closure that the alpha time is directly related to a thermodynamic property⁵⁰, our present results suggest a new direct relationship between the matrix alpha time and the short time scale in pure hard sphere fluids.

B. Degree of Decoupling of the Penetrant Hopping Time from the Matrix Alpha Relaxation Time

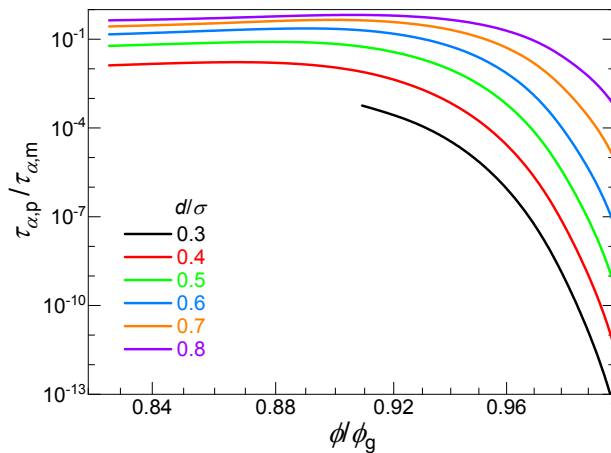


Fig.5 Degree of decoupling as quantified by the ratio of the penetrant to matrix alpha times plotted as a function of packing fraction scaled by its value at the matrix kinetic glass transition relevant to thermal liquids ($\phi_g \sim 0.605$). For colloidal suspensions which kinetically vitrify at $\phi_g \sim 0.58-0.59$ the x-axis would not exceed $\sim 0.96-0.975$. Termination of the black curve for the smallest penetrant fraction reflects dynamic localization is not predicted by NMCT at sufficiently low matrix packing fraction.

Beyond very small penetrant displacements, transient localization emerges in a dense matrix, resulting in long time penetrant motion becoming activated and coupled to a variable

degree with matrix displacements. Many new questions then arise. In this subsection we consider the degree to which penetrant hopping requires a correlated matrix displacement, which we refer to as the amount of coupling or decoupling. This question can be mechanistically studied using distinct physical metrics.

As readily probed in experiment or simulation, one characterization of the degree of decoupling as the ratio of the penetrant to matrix alpha relaxation times. Results for this quantity are shown in Fig. 5 as a function of scaled effective packing fraction at variable penetrant sizes. As expected, the degree of decoupling increases (smaller time ratio) monotonically with penetrant size. However, its matrix packing fraction dependence is subtle, with the time ratio first increasing slowly with ϕ , and then sharply decreasing. Hence, an interesting (albeit weak) non-monotonic evolution of the time ratio in Fig. 5 with matrix packing fraction is predicted. With decreasing penetrant size (and hence a larger time scale separation between penetrant hopping and the matrix alpha process), this non-monotonic behavior eventually disappears. With the goal of developing a microscopic understanding of the origin of this behavior, we first analyze the key properties that determine the penetrant total barrier and alpha time.

The *absolute* magnitudes of the penetrant jump distance and its correlated matrix displacement as a function of size ratio are shown in Fig.SI2, with the following salient features evident. The penetrant jump distance varies non-monotonically with size ratio, first increasing, and then going through a maximum at a size ratio that depends weakly on matrix packing fraction ($d \sim 0.35-0.45\sigma$), followed by a decrease. In contrast, the correlated matrix displacement $\Delta r_{m,c}$ grows monotonically at low and medium values of d/σ , gradually approaching a plateau (saturation) value which is almost identical to the jump distance of the *pure* matrix alpha relaxation event. These trends imply penetrant hopping becomes more strongly coupled with the

matrix alpha relaxation as it grows in size, approaching a “slaved” limit of full coupling for large enough penetrants, as further discussed in the SI.

The above results imply that small enough penetrants can hop without requiring much matrix motion. If so, then their activated hopping event is largely *noncooperative* in the sense of being dominated by the local cage barrier. This physical picture is supported by the numerical calculations in the inset of Fig. 6 of the ratio of the local cage dynamic free energy cost for the correlated matrix displacement, $F_{B,m,c}$, to its pure matrix analogue for its full alpha process, $F_{B,m}$. Physically, the former is the dynamical cost for matrix particles to displace “uphill” via thermal fluctuation on their dynamic free energy in order to facilitate penetrant hopping. At low d/σ , this ratio is well below unity and increases linearly with size ratio. Hence, the correlated matrix displacement ($r_{m,c}$) in this regime is *not* associated with matrix particles reaching their dynamic free energy barrier per a matrix structural relaxation event. However, as the size ratio becomes sufficiently large the barrier ratio approaches unity, and thus the matrix is required to undergo its own alpha relaxation event to allow the penetrant to hop corresponding to maximal penetrant-matrix coupling or “slaving”. Interestingly, to leading order the d/σ -dependences of $F_{B,m,c}/F_{B,m}$ collapse for different packing fractions, corresponding to the degree of decoupling being set mainly by the geometric size ratio d/σ .

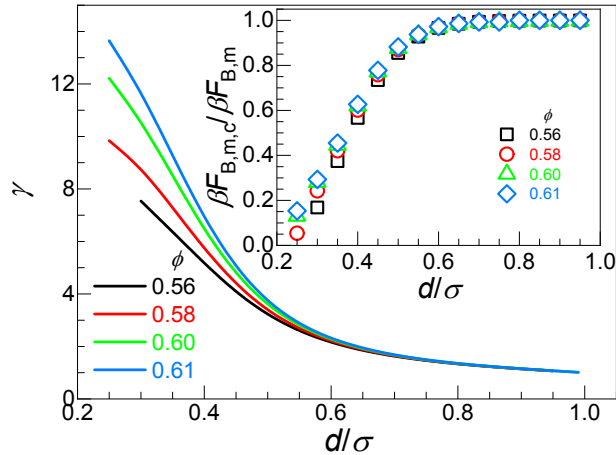


Fig. 6 Main: Self-consistently determined dynamic coupling parameter γ as a function of size ratio for various matrix packing fractions. Inset: Ratio of the dynamic free energy cost associated with correlated matrix displacement to the full cage barrier of the pure matrix fluid as a function of size ratio for various matrix packing fractions.

Further insight concerning decoupling follows from consideration of the magnitude of the penetrant hopping displacement *relative to* its correlated matrix analogue. By construction, this is the fundamental quantity of the SCCH theory -- the temporally self-consistent coupling parameter, γ . The main frame of Fig. 6 presents calculations as a function of penetrant size for various matrix packing fractions; the results exhibit the same *qualitative* trends found previously based on using OZ-PY structural input³². The parameter γ sensibly increases as penetrants become smaller (more decoupling, less matrix participation in penetrant hopping). On the other hand, a slaved limit (full coupling, $\gamma \rightarrow 1$) is approached in a matrix packing fraction *insensitive* manner when $d \sim 0.6\sigma$ (which is where $\Delta r_{m,c}$ enters the plateau regime, see Fig. SI2). This onset of slaving as deduced from γ will be shown in the next subsection to be tightly correlated with the breakdown of an exponential dependence of the penetrant alpha time on size ratio.

Finally, we return to the weak *non-monotonic* dependence of decoupling in Fig. 5. The surprising result is that with increasing matrix packing fraction the degree of decoupling first

modestly *decreases*. The reason is that at lower ϕ the penetrant barrier to hopping is relatively low and dominated by its local cage component, and hence the penetrant relaxation time is more strongly affected by the non-activated short time process discussed in sub-section IIIA. The latter timescale (or short time friction) is predicted to *grow faster* with packing fraction than its pure matrix analogue, resulting in the net trend of weakly less decoupling. But at higher ϕ , penetrant and matrix barriers become larger, and the short time scale process becomes of minor importance. Most importantly then is that the elastic barrier associated with the matrix alpha process grows more rapidly with increasing ϕ than its analogue associated with facilitation of the penetrant hopping event which involves a relatively smaller matrix displacement. This results in the relaxation time ratio in Fig. 5 strongly decreasing, and more so as packing fraction further grows, thereby yielding the non-monotonic dependence in Fig. 5.

C. Size Ratio Dependence of Penetrant Relaxation Time

The prior SCCH theory study³² based on using the PY closure for structure discovered a roughly exponential dependence of the penetrant diffusion constant (inverse relaxation time) on *one power* of d/σ that covered ~ 9 decades *at* the matrix glass transition for $d/\sigma = 0.3-0.9$ (see Fig.SI3). A qualitatively similar exponential dependence has been observed in simulations^{14, 21, 22, 46} for the penetrant diffusion constant in polymer matrices covering ~ 4 decades variation.

Figure 7 presents new calculations of the penetrant alpha time (scales as the inverse diffusion constant³²) as a function of penetrant size ratio for various packing fractions (corresponding to a very wide range of matrix alpha times) using the MV closure for structural correlations. A linear exponential growth is again found, which applies over a specific size ratio regime that grows significantly with matrix packing fraction. However, it holds to an even better degree than the prior PY based computations, now covering more than 16 decades at $\phi = 0.61$

(~laboratory matrix glass transition for a viscous liquid) for the entire penetrant size range ($d/\sigma = 0.25-1.0$). This is a striking explicit example of how the range of applicability of a predicted qualitative dynamic behavior can be strongly changed by using more accurate structural input. Now, with decreasing packing fraction (maps to higher temperatures in viscous liquids), such an exponential dependence, $\tau_{\alpha,p} \sim e^{b(d/\sigma)}$, holds over an increasingly narrower range of size ratios and with a significantly lower slope parameter ($b \sim 25.55, 34.6, 41.7,$ and 54.0 for $\phi=0.56, 0.58, 0.6,$ and 0.61 , respectively). Thus, we conclude that the exponential size ratio dependence is a subtle effect that depends on matrix thermodynamic state and proximity to its glass transition. To incisively test our results in Fig. 7 requires new simulations performed over a wide range of size ratios and matrix packing fractions or temperatures. Further discussion of a very recent simulation study¹⁴ that is highly germane to these theoretical results is given in sub-section VB.

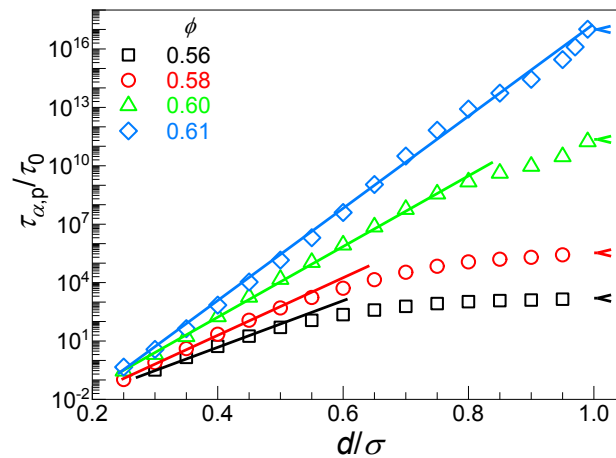


Fig. 7 Penetrant alpha relaxation time (in units of τ_0) as a function of size ratio for various matrix packing fractions. Arrows indicate the corresponding matrix alpha times, which map crudely to specific times in seconds for viscous liquids and colloidal suspensions as explained in Fig.1. Lines indicate an effectively linear behavior which applies over an increasing number of decades of relaxation time as matrix packing fraction (or alpha time) grows.

The question now is what is the mechanism underlying the rich behavior in Fig. 7 and the precise origin of an exponential growth law? Ultimately, the answer lies in the size ratio and matrix packing fraction dependences of the penetrant local cage, elastic, and total barriers, which are individually shown in Fig. 8a for $\phi = 0.61$. One sees that elasticity effects are negligible at low size ratios, and the cage barrier increases linearly with size ratio, reaching a plateau starting at $d \sim 0.6\sigma$, as expected based on the results in Section IIIB. Moreover, the local cage components of the dynamic free energy cost for the penetrant and matrix, $F_{B,p}$ and $F_{B,m,c}$, are very close for all size ratios. This prediction emerges from the temporal self-consistency condition of SCCH theory. Given we also know there is a crossover at $d \sim 0.6\sigma$ to slaved motion, one can conclude that the appearance of a plateau in $F_{B,p}$ is due to this physical behavior. Curiously, Fig. 8a also shows that the slope of the penetrant *cage* barrier versus d/σ plot in the *lower* size ratio regime (where it dominates the total barrier) is nearly identical to that of the elastic barrier that dominates in the *high* d/σ regime. This behavior in the glass-like matrix at $\phi = 0.61$ is the origin of the nearly *linear* relationship between the total barrier and d/σ over *all* size ratio regimes. Hence, we deduce there is a subtle compensation effect for the physically relevant *total* barrier underlying the exponential growth of the penetrant relaxation time with d/σ .

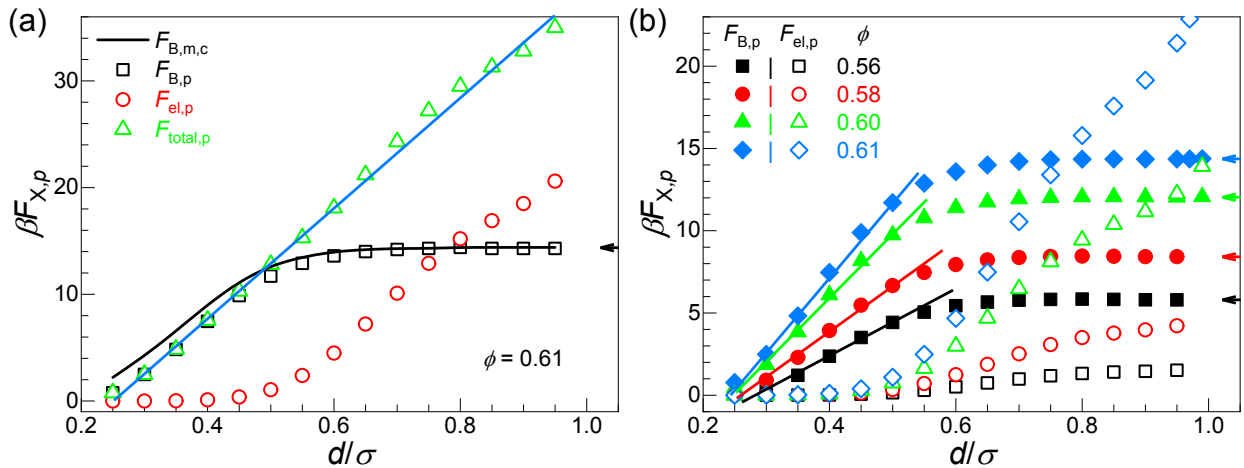


Fig. 8 (a) Penetrant cage (square), elastic (circle), and total (triangle) barriers as a function of size ratio at a very high packing fraction ($\phi = 0.61$). The corresponding dynamic free energy cost of the correlated matrix displacement ($F_{B,m,c}$) from $r_{loc,m}$ to $r_{m,c}$ is shown as the solid black curve. (b) Penetrant cage (solid) and elastic (open) barriers as a function of size ratio for various matrix packing fractions. Arrows indicate the corresponding matrix local cage barriers.

Figure 8b examines how the above compensation effect changes at lower matrix packing fractions relevant to glass forming viscous liquids above (and approaching) their T_g or dense equilibrated colloidal suspensions below (and approaching) ϕ_g . One sees that although it also holds at $\phi = 0.6$, it is not accurate over the entire size ratio range. In the high d/σ regime, the slope corresponding to the elastic barrier slightly decreases. As the packing fraction further decreases, the elastic barrier eventually becomes smaller than its cage analogue beginning in the plateau regime of the cage barrier, resulting in a saturation of total barrier (i.e., the breakdown of the strict compensation effect that underlies the exponential behavior of the penetrant alpha time) for large enough size ratios. Thus, the compensation effect is a delicate balance of factors which accurately holds to a degree in d/σ space that depends on ϕ and hence matrix dynamics. Since the relaxation time is proportional to the exponential of the total barrier, as one sees in Fig. 7 the compensation effect (and hence exponential growth) is predicted to effectively disappear at the lowest packing fraction studied. Future experiments and simulations performed at relatively lower packing fractions or higher temperatures over a wide range of size ratios can test this scenario.

D. Dependence of Penetrant Hopping on Matrix Packing Fraction

Finally, we consider the evolution of the penetrant alpha time with matrix packing fraction at fixed size ratio, d/σ . Fig. 9 shows the results. In the lower packing fraction regime of $\phi < 0.56$ (maps to higher temperature for viscous liquids, recall Figure 1), the matrix elastic barrier is negligible, and the penetrant alpha time increases only slightly for all penetrant size ratios. But

for higher packing fractions germane to deeply supercooled liquids or highly metastable colloidal suspensions ($\phi > 0.56$), the penetrant alpha time grows significantly with ϕ , and increasingly so for larger penetrants, due to collective elasticity effects. Overall, the increase is rather remarkably weak for smaller penetrants (< 4 decades when $d < 0.5$), due to the strong “decoupling” between penetrant and matrix dynamics. Note that no linear behavior is found between the logarithm of the penetrant alpha time and packing fraction, and thus no “generalized Arrhenius” regime exists for penetrant activated relaxation.

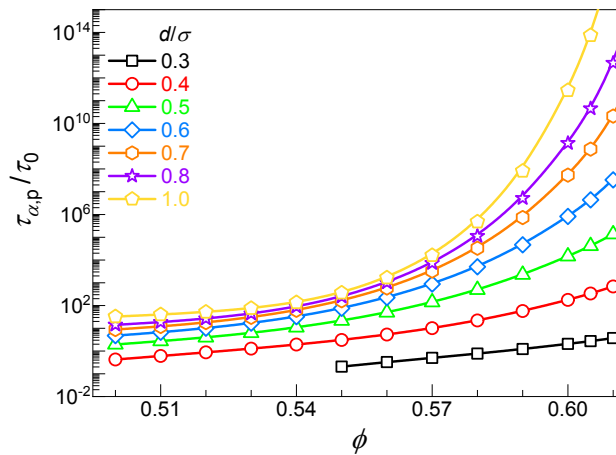


Fig. 9 Penetrant alpha relaxation time (in units of τ_0) as a function of matrix packing fraction for several size ratios d/σ including the pure matrix result ($d/\sigma = 1$). Termination of the black curve for the smallest penetrant reflects dynamic localization is not predicted by NMCT at sufficiently low matrix packing fraction.

To better understand the matrix packing fraction dependences in Fig.9, we consider in detail what factors determine the penetrant collective elastic barrier. Per eqn (17), the question is the relative importance of the self-consistently determined matrix displacement that sets the amplitude of the elastic field, versus the contribution from harmonic curvature of the *pure* matrix dynamic free energy (proportional to the matrix dynamic shear modulus, G'). Fig. SI4 shows the latter increases exponentially with packing fraction, and is always the primary factor that

determines the elastic barrier, regardless of size ratio, although the contribution of the matrix displacement that enters as $\Delta r_{m,c}^4$ in the elastic barrier is not negligible.

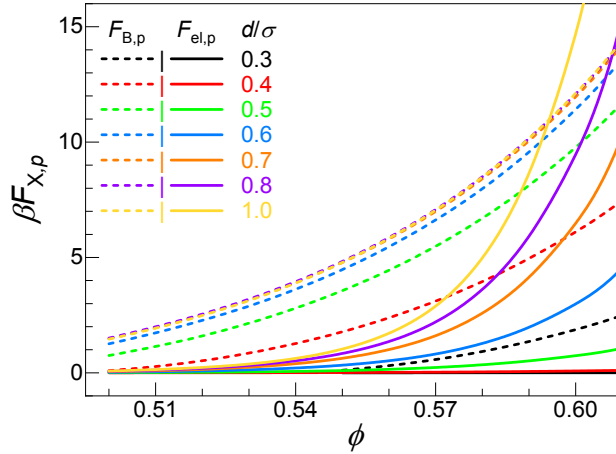


Fig. 10 Penetrant cage (short-dash) and elastic (solid) barriers as a function of matrix packing fraction for a series of size ratios.

Of most direct relevance to the behavior in Fig.9 is the packing fraction dependence of the penetrant cage and elastic barriers for a range of size ratios which are shown in Fig. 10. In the lower d/σ regime, the elastic barrier is negligible, and the cage barrier determines the penetrant relaxation time. Because the cage barrier remains relatively small with increasing ϕ , the penetrant alpha time in the low d/σ regime increases only slightly with packing fraction. However, in the high d/σ regime the elastic barrier becomes very significant, and ultimately dominates the penetrant relaxation time at high packing fractions, resulting in a major increase of penetrant relaxation time with ϕ .

IV. Connections to Matrix Short Time Dynamics and Thermodynamics

There is a long history for the problem of structural relaxation in glass forming liquids of searching for a “correlation” between slow dynamics (alpha relaxation time) and a specific thermodynamic property or a simple metric of short time relaxation. Whether such connections

are unique, let alone causal, continues to be vigorously debated. In this section we consider this issue for the new problem of activated penetrant relaxation and transport. Shedding light on this question is not only of scientific interest, but also has the potential to influence experimental work and materials design if penetrant mobility can be reliably predicted from knowledge of equilibrium properties and/or short distance/time dynamics.

We begin by noting that for *one*-component HS fluids the present dynamical theory with PY-based structural input predicts a simple relation between the (transient) localization length and local cage barrier^{37, 57}, $\beta F_B \propto \sigma/r_{\text{loc}}$. Does the analogue of this connection between an activation barrier and a short time/length scale dynamical property exist for the penetrant problem? This new question is answered in the inset of Fig. 11 using MV structural input. Rather surprisingly, the penetrant cage barrier is an excellent linear function of the inverse penetrant localization length over a wide range of matrix packing fractions for all penetrant sizes, albeit with a slope that varies with size ratio and with some deviations at very high packing fraction for larger penetrants. Beyond the intrinsic interest of a connection of the local activation barrier with a short time dynamic localization property, recall that at low d/σ the cage barrier dominates the penetrant hopping time. As such, we can conclude that the NMCT transient penetrant localization length^{31, 37, 38} essentially fully determines penetrant activated relaxation and transport in the low d/σ regime. This striking prediction is potentially testable in experiment and simulation since the transient dynamic localization length can be extracted from measurements of the single particle mean square displacement or incoherent dynamic structure factor in an appropriate wavevector and temporal regime.

An important thermodynamic property of the pure matrix (which is straightforwardly measurable in both simulation and experiment) is the inverse dimensionless compressibility^{47, 48}.

It also quantifies the amplitude of long wavelength density fluctuations, and is intimately connected to an integrated measure of equilibrium packing correlations embedded in $g(r)-1$. Prior ECNLE theory studies of one-component hard sphere fluids⁵⁰ found a linear correlation between the local cage barrier and inverse dimensionless compressibility, $1/S_0$. Fig. 11 presents calculations that test this connection for the *penetrant* local cage barrier. The latter changes a lot with penetrant size, though (of course) the *matrix* inverse dimensionless compressibility remains the same since the penetrant is at infinite dilution. Rather surprisingly, we find a good linear correlation between this penetrant local dynamic property and a thermodynamic property of the pure matrix, even when penetrants are sufficiently large ($d/\sigma > 0.5-0.6$) that their dynamics is strongly affected by elasticity effects. This linear correlation works even better than seen in the inset of Fig. 11 for larger penetrants ($d/\sigma > 0.5-0.6$).

The experimental and simulation relevance of the results in Fig.11 lies in the theoretical prediction that when penetrants are sufficiently *small* the elastic barrier is negligible and the local cage barrier determines its alpha relaxation time and diffusion constant. Hence, Fig.11 implies an exponential connection between the penetrant alpha time and matrix inverse dimensionless compressibility, as shown in Fig. 12a. More generally, it is well established for one-component fluids⁴⁸ that the inverse dimensionless compressibility is proportional to square of other structural length scales (or order parameters) directly determined by the pure matrix pair correlation function $g(r)$ or static structure factor $S(q)$. Hence, we conclude that strong connections also exist between penetrant dynamics and matrix structural correlation lengths, a nontrivial mechanistic insight.

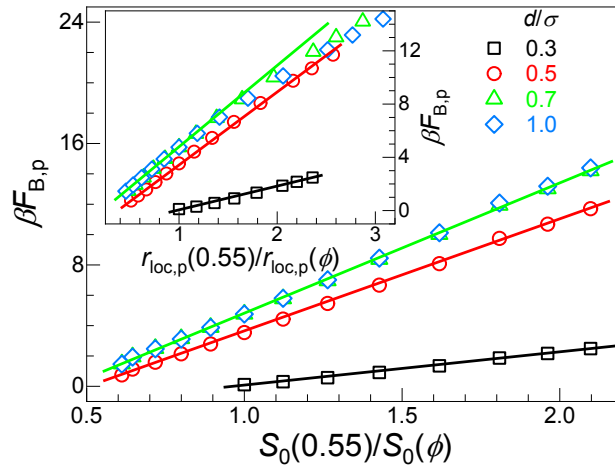


Fig. 11 Penetrant cage barrier as a function of scaled inverse matrix dimensionless compressibility (main) and inverse penetrant localization length scale (inset) for a wide range of matrix packing fractions (0.5-0.61) and several size ratios.

Now, with increasing penetrant size its motion is predicted to be increasingly coupled with matrix elasticity, and both the local cage and collective elastic barriers are crucial in determining the penetrant hopping rate. This is evident from the failure of the exponential relation in Fig. 12a for $d/\sigma > 0.5-0.6$, which becomes increasingly apparent at higher matrix packing fractions (smaller S_0 , higher bulk modulus). As known from our recent ECNLE theory analysis⁵⁰ of one-component metastable hard sphere fluids, when the elastic barrier is important a distinctive compensation-like effect between changes of the local cage and elastic barrier contributions to the total barrier emerges, resulting in the prediction that the *total* barrier (or logarithm of the alpha time) scales as the inverse *cube* of the dimensionless compressibility.

Figure 12b tests whether the above behavior applies to the problem of penetrant activated relaxation. Again, rather surprisingly and remarkably, one sees that it does hold quite well, albeit to a variable degree depending on the value of d/σ and range of matrix packing fractions considered. The higher the packing fraction, the more important collective elasticity is for matrix dynamics, although the degree to which penetrant motion couples to matrix elasticity decreases as penetrants become smaller. We also note that even when the cubic scaling applies, the slope

grows with penetrant size. This reflects the increased coupling of its motion to the matrix, and the growing extent to which the matrix alpha relaxation process is required to allow larger penetrants to hop. Defining a slope from the plot of the logarithm of the penetrant alpha time versus cubic inverse dimensionless compressibility as $k_{\tau_\alpha-S_0^{-3}}$, we find (not plotted) an excellent power law relation holds, $k_{\tau_\alpha-S_0^{-3}} \approx 24.76(d/\sigma)^{3.24}$. A simple interpretation of this result seems difficult given the coupled and self-consistent nature of the penetrant plus correlated matrix dynamic fluctuation event.

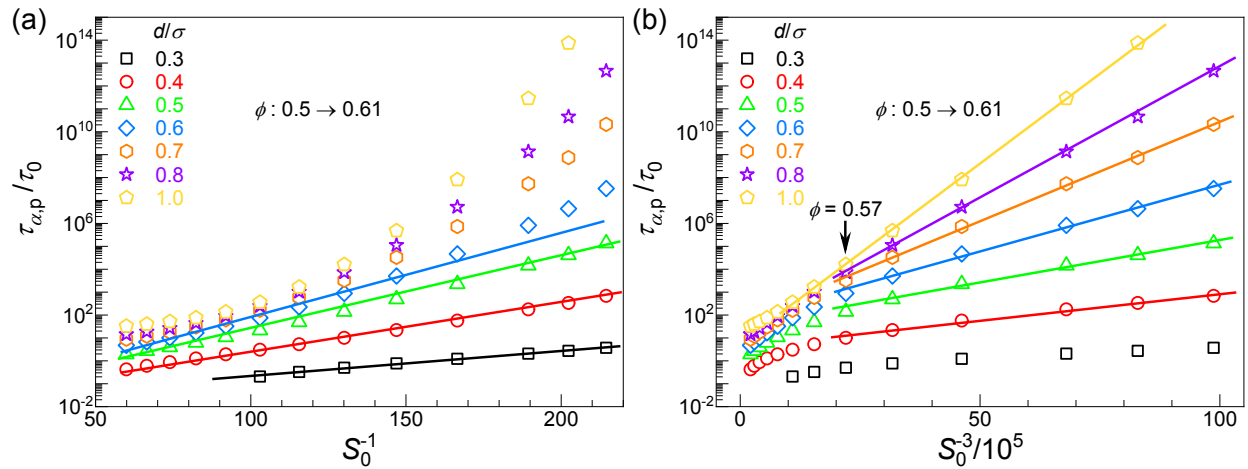


Fig. 12 Penetrant alpha time (unit of τ_0) as a function of inverse matrix (a) dimensionless compressibility, and (b) cubed dimensionless compressibility, for several size ratios.

Thus, we conclude that the SCCH theory with accurate structural input *does* predict direct connections exist for penetrant mobility with specific equilibrium structural and thermodynamic quantities. Moreover, for relatively small penetrants, a causal connect also exists with the classic metric of small scale caging, the penetrant dynamic localization length.

V. Summary of Key Predictions and Comparisons with Simulation

A. Key Predictions for Viscous Liquids and Colloidal Suspensions

With the goal of stimulating new experimental and simulation tests of our theory, we briefly summarize key testable predictions based on our analysis of a spherical tracer in a hard sphere matrix model. (1) Figure 4 predicts a size ratio invariant power law growth (decrease) of the non-activated process short relaxation time (short time diffusivity) with the penetrant-matrix contact value to the $7/3$ power over a wide range of matrix packing fractions. (2) Figure 5 predicts a weakly non-monotonic, size ratio dependent evolution of the degree of dynamic decoupling (defined as the ratio of the penetrant to matrix long time alpha times or inverse diffusion constants) with packing fraction. Non-dimensionalization of matrix packing fraction by its kinetic glass transition value is a practical route to mapping the theoretical results onto real world systems. (3) Figure 7 predicts how the penetrant alpha time or inverse diffusion constant grows with size ratio in a packing fraction dependent manner (from the weakly supercooled to glass regimes). This includes the range of exponential scaling and the associated pre-factor in the exponential which can be thought of as defining the relevant matrix length scale (see next section), and the tendency to bend over or saturate for “large enough” size ratio. (4) Figure 12 predicts two distinct exponential regimes of growth (decay) of the penetrant relaxation time (inverse diffusivity) with the experimentally measurable inverse thermodynamic dimensionless compressibility of the pure matrix raised to the 1 or 3 power depending on size ratio and how slow the matrix alpha relaxation is.

Given the previously demonstrated ability within ECNLE and SCCH theories to map molecular viscous liquids to effective hard sphere fluids, the above key predictions should also be qualitatively testable for spherical atoms or weakly non-spherical molecules in thermal liquids. We now turn to a specific example of this relevance.

B. Penetrants in Viscous Liquids

Very recently, a comprehensive simulation study of atomic and molecular penetrants of variable shape and size in a cold polymer liquid ($T/T_{g,\text{matrix}} \sim 1.2$) was performed¹⁴. For spherical atomic and nearly spherical molecular penetrants, their diffusivity was found to follow a simple exponential law in penetrant diameter, $D \propto e^{-d/\lambda}$; alternative free volume and other models^{15, 16} predict an exponential dependence but with the penetrant diameter squared or cubed, which clearly fail. For the simulated high polymer matrix packing fraction of $\phi \sim 0.59$, the length parameter was very small, $\lambda \sim 0.019$ nm.

This exponential behavior¹⁴ is in excellent agreement with our theoretical results, as was discussed in detail by the authors of the simulation study of ref.14. Quantitatively, from subsection IIIC and Fig. 7, we expect that at $\phi \sim 0.59$ the length parameter is $1/b \sim \sigma/38$. Based on the established mapping adopted in ECNLE theory for polymer liquids, the matrix spherical particle diameter corresponds to a volume equal to a Kuhn length of the polymer chain.^{64, 65} Its characteristic size for many polymers is ~ 1 nm, consistent with the simulation parameter¹⁴. Hence, the theory anticipates $\lambda \sim 1/38$ nm ~ 0.026 nm. Given the theory employs an effective hard sphere mixture model, versus the atomistic description of atomic and molecular penetrants in a polymer liquid in the simulation¹⁴, we find this level of agreement very encouraging.

Clearly more simulations are required. For example, even for the model of ref.14, if one changes T/T_g (effectively ϕ) then other predicted aspects in Fig. 7 can be tested. This includes the evolution of the strength of the exponential behavior, its range of validity in size ratio space, and the tendency to saturate. These issues are further discussed in the next sub-section for tracer hard sphere diffusion in dense hard sphere matrices, which connects with key prediction (3) in subsection VA. New simulations should also be able to test predictions (2) and (4), and even (1).

C. Tracer Relaxation in Dense Colloidal Matrices

Recently, simulations²⁹ of the alpha relaxation time of tracer hard spheres in dense (glassy) hard sphere fluids (slightly polydisperse) of larger particles have been performed that are directly relevant to our theoretical work. The (mean) size ratios simulated that are relevant to our study is $d/\sigma = 0.5-1$, and the matrix packing fraction was fixed at $\phi = 0.59$. Although modest aging effects were evident, after very long waiting times the penetrant alpha times were found (see Fig. 13a) to be nearly equilibrated, and grow by ~ 2.5 decades²⁹ over the range $d/\sigma = 0.5-1$. Figure 13a shows the simulation data (at the longest waiting time) follows a roughly exponential growth at lower size ratios, and then bends over to a weaker dependence. These behaviors are in excellent qualitative accord with our calculations in Fig. 7. We note that complementary dynamic x-ray experiments were also performed²⁹.

Figure 13a also represents a quantitative comparison of our theory with the simulation study for the *shape* of how the tracer relaxation time grows with size ratio. A small ambiguity is the appropriate value of matrix packing fraction in the theory which employs a monodisperse hard sphere model. It is well known polydispersity speeds up dynamics, and hence the appropriate ϕ should presumably be slightly smaller than 0.59. Calculations for packing fractions of 0.58, 0.585 and 0.59 are shown in Fig. 13a. The perhaps most sensible choice of 0.58 results in quantitative agreement between theory and simulation. Given the simulation and theory models are almost identical, this agreement seems very significant. New simulations of the same model can be designed to critically test the predicted evolution of the behavior in Fig.7 for higher and low packing fractions.

The same simulation study²⁹ extracted a penetrant transient dynamic localization length ($r_{loc,p}$ in our language) from the wavevector (found to be Gaussian, per the theory eqn (9))

dependence of the penetrant incoherent dynamic structure factor. These simulation results did not show significant aging effects. The results in the range $d/\sigma = 0.5-1$ are shown in Fig. 13b, along with one experimental point²⁹. The data roughly follow an inverse power law scaling, albeit with deviations as the penetrant size approaches that of the matrix particles. Also shown is our theoretical prediction, which follows an excellent power law, $r_{\text{loc,p}}/\sigma \propto \phi^{-y}$, with $y \sim 1.67-1.75$ over the range $\phi = 0.56-0.61$. Overall, one sees good agreement between theory and simulation for the size ratio dependence (*no fitting is involved*). A possible caveat is that we have only computed the localization length as analytically estimated via the minimum of the penetrant dynamic free energy in Fig.2, while simulations extract it from a full dynamic calculation of a time-dependent structure factor. This difference may account for the mismatch in absolute values of the theoretical and simulated localization lengths.

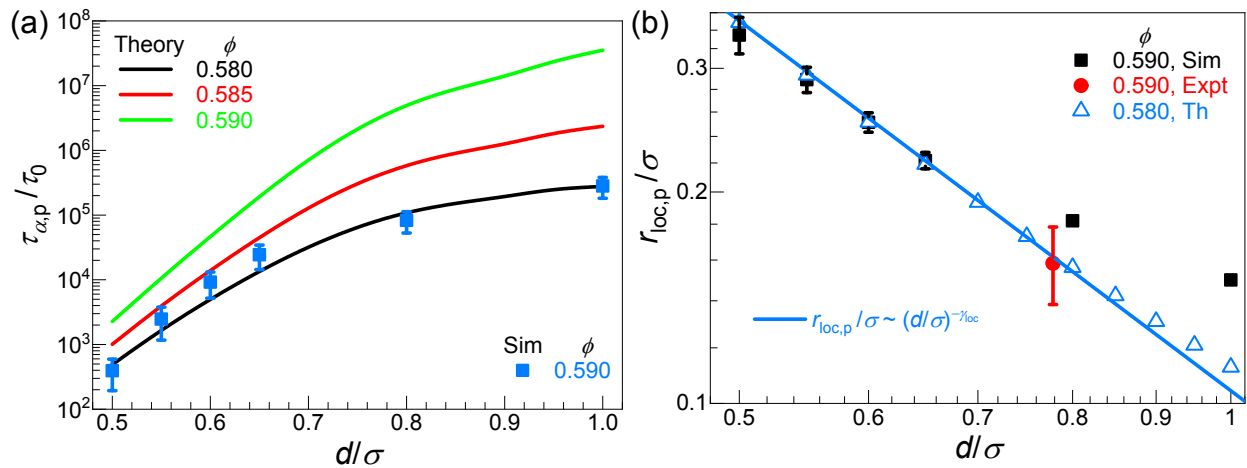


Fig. 13 (a) Penetrant mean alpha relaxation time (in units of τ_0 for our theory and $t_s = \sigma(m/k_B T)^{1/2}$ for simulation²⁹) as a function of size ratio. Curves are the same theoretical results as in Fig. 7 but plotted for packing fractions of 0.58, 0.585, and 0.59. Points are the simulation data at $\phi = 0.59$. (b) Theoretical localization length (blue triangles) as a function of size ratio at $\phi = 0.58$ (shifted up by a factor of 7), and corresponding simulation results (black squares) and a single experimental data point²⁹.

VI. Summary and Future Directions

We have employed the self-consistent cooperative hopping (SCCH) theory³² for dilute penetrant motion in very dense hard sphere fluid matrices to address multiple new questions and make testable predictions over a wide range of packing fractions (in the metastable regime) and penetrant-to-matrix size ratios. Our results are relevant to both dense colloidal suspensions and supercooled viscous liquids. A technically new aspect is the use of a much improved description of packing correlations (MV closure) which plays a central role in constructing the coupled penetrant and matrix dynamic free energies from which correlated activated dynamics is predicted. Four main topics were studied: (i) the short time/distance penetrant relaxation time associated with non-activated dynamics; (ii) decoupling and slaving between the penetrant activated hopping rate and the matrix alpha relaxation; (iii) the physical mechanism that underlies the extent and precise form of the matrix packing fraction dependent exponential relationship between penetrant mobility and size ratio; (iv) discovery of a new relationship between the equilibrium thermodynamic dimensionless compressibility with the penetrant relaxation time and diffusion constant. We also compared some of our results with recent simulations on tracer diffusion and transient localization in dense colloidal suspensions and viscous liquids, which appear to provide significant support for the theoretical ideas. Below we recap the highlights from each of these areas.

The non-activated short time/distance penetrant relaxation time, $\tau_{s,p}$, quantifies the initial fast dissipative process, and also sets the timescale for the slower penetrant hopping process. A generic power law scaling of this time scale with the contact value of the penetrant-matrix pair correlation function, g_{mp}^{contact} , with an exponent of 7/3 was predicted, and its origin understood. In

the lower matrix packing fraction regime where cage barriers are modest and collective elasticity effects unimportant, the penetrant dynamics can be dominated by $\tau_{s,p}$.

As matrix packing fraction or penetrant size grows, high barriers emerge, and ultimately the collective elasticity cost associated with the correlated matrix fluctuation that facilitates penetrant hopping becomes dominant. The amplitude of the required matrix dynamic fluctuation increases as penetrants become larger. These features conspire to result in a rich dynamic decoupling behavior. Their interplay underlies our discovery of a weakly non-monotonic variation with matrix packing fraction of the decoupling ratio $\tau_{\alpha,p}/\tau_{\alpha,m}$, which is causally related to the self-consistently determined relative displacement parameter γ . Beyond $d \sim 0.6\sigma$, a strong coupling or slaving of penetrant hopping and the facilitating matrix dynamic fluctuation emerges. It can be understood as when the ratio of the cage dynamic free energy cost of the correlated matrix fluctuation to its value for a full matrix alpha relaxation event, $F_{B,m,c}/F_{B,m}$, approaches unity. This limiting behavior is essentially independent of matrix packing fraction, thereby emphasizing the crucial role of the geometric factor d/σ in determining the degree of decoupling and ultimately slaving between matrix and penetrant.

How matrix collective elasticity affects penetrant hopping depends strongly on penetrant size via the magnitude of the facilitating matrix displacement ($\Delta r_{m,c} = \Delta r_p/\gamma$) and the matrix shear rigidity. The latter always grows with packing fraction, while the former is nearly independent of ϕ in the lower d/σ regime, but increases with packing fraction in the larger d/σ regime. We predict that matrix elasticity is unimportant for small enough penetrants ($d < 0.6\sigma$), but increasingly dominant for larger ones, in a manner that quantitatively depends on matrix packing fraction. Based on a detailed analysis of the absolute and relative contributions of local cage to collective elastic barriers that resist penetrant motion, we established a mechanistic

understanding of the exponential growth of the penetrant relaxation time with size ratio that emerges at very high packing fractions. We conclude it is a subtle compensation effect, which also explains its continuous breakdown as penetrants become larger and/or the matrix packing fraction becomes low enough.

We explored possible connections between the penetrant hopping time and a key thermodynamic property that quantifies long wavelength thermal density fluctuations of the matrix – the inverse dimensionless compressibility, $1/S_0$. When collective elasticity is unimportant (small penetrants and/or lower matrix packing fraction), the penetrant total barrier scales linearly with $1/S_0$. However, when collective elasticity plays an important role in the dynamic free energy cost of a facilitating matrix displacement, the penetrant total barrier is predicted to scale as the 3rd power of $1/S_0$. These intriguing findings, though only deduced for systems that interact via hard core repulsions, have major implications. For example, a surprising causal connection is suggested between penetrant relaxation time or diffusivity with a *pure* matrix thermodynamic property that can be determined experimentally from equation-of-state measurements. We urge new simulation and experimental studies be performed to test this result, which could also be of major value in functional soft materials applications and design.

Finally, we comment on the many possible future directions. The combination of integral equation theory, ECNLE theory, and SCCH theory can be extended to address the rich complexity of activated penetrant dynamics in real systems and materials over an enormous range of timescales based on much prior work by Schweizer and coworkers. For spherical particle models, one can easily take into account non-hard core repulsions (e.g., a soft repulsive Hertzian potential relevant to microgels^{66, 67}), strong short range attractions (physical bonds) between matrix particles resulting in dense gel or attractive glass matrices^{68, 69}, and penetrant-

matrix attractions relevant to specific physical bonding or association forces^{32, 65}. The theoretical tools also exist to address non-dilute mixtures of spherical particles, as recently done under purely hard core repulsion conditions⁴². This advance allows questions such as single versus double glass formation, and plastization versus anti-plastization, to be studied⁴². From a theoretical methods perspective, the dynamic free energy approach can be potentially implemented at the stochastic trajectory level per prior work^{39, 40}. This would allow the calculation of the time-dependent mean square displacement, non-Gaussian parameters, and all other single particle time correlation functions, including aspects of dynamic heterogeneity. Building on prior advances, extension of the theory penetrant dynamics at the quasi-analytic level employed in this article is also possible in order to address the impact of nonspherical penetrant shape^{70, 71}, connected semiflexible polymer chain matrices^{72, 73}, polymeric crosslinking⁷⁴, and quenched (pinning) disorder in colloidal systems⁷⁵. The influence of applied stress or strain on penetrant dynamics can be treated based on the well-developed nonequilibrium version of the dynamic free energy concept^{76, 77}.

The above generalizations will further broaden the relevance of the theoretical approach to experimental and simulation studies, and also help guide soft materials development. The latter potentially includes membrane separation science where the permeability is the product of penetrant solubility and diffusion constant^{5, 8, 11}. Penetrant solubility can be determined using equilibrium integral equation theory methods, and combined with the present approach for the penetrant relaxation time and diffusivity. One can also employ the developed mapping from hard sphere models to viscous liquids^{34, 64, 65} to explicitly address experiments on specific molecular and polymer systems where temperature is the control variable. Work in many of these directions is underway.

Acknowledgement

We acknowledge support from DOE-BES under Grant DE-FG02-07ER46471 administered through the MRL at UIUC. Stimulating discussions and technical assistance in the early stages of this work with Drs. Rui Zhang and Shi-Jie Xie are gratefully acknowledged.

Conflicts of Interest

There are no conflicts to declare.

References

- 1 M. T. Cicerone, F. Blackburn and M. Ediger, *J. Chem. Phys.*, 1995, **102**, 471.
- 2 S. C. George and S. Thomas, *Prog. Polym. Sci.*, 2001, **26**, 985.
- 3 J. Guan, B. Wang and S. J. A. n. Granick, *ACS Nano*, 2014, **8**, 3331.
- 4 K. Paeng, H. Park, D. T. Hoang and L. J. Kaufman, *Proc. Natl. Acad. Sci. USA*, 2015, **112**, 4952.
- 5 J. S. Vrentas and C. M. Vrentas, *Diffusion and mass transfer*, CRC Press, Boca Raton, 2016.
- 6 D. F. Sanders, Z. P. Smith, R. Guo, L. M. Robeson, J. E. McGrath, D. R. Paul and B. D. Freeman, *Polymer*, 2013, **54**, 4729.
- 7 M. Galizia, W. S. Chi, Z. P. Smith, T. C. Merkel, R. W. Baker and B. D. Freeman, *Macromolecules*, 2017, **50**, 7809.
- 8 W. J. Koros and R. Mahajan, *J. Membrane Sci.*, 2000, **175**, 181.
- 9 J. F. Patrick, M. J. Robb, N. R. Sottos, J. S. Moore and S. R. White, *Nature*, 2016, **540**, 363.
- 10 B. J. Blaiszik, S. L. Kramer, S. C. Olugebefola, J. S. Moore, N. R. Sottos and S. R. White, *Ann. Rev. Mater. Res.*, 2010, **40**, 179.
- 11 G. M. Geise, D. R. Paul and B. D. Freeman, *Prog. Polym. Sci.*, 2014, **39**, 1.
- 12 J. Vrentas and J. Duda, *J. Polym. Sci. B-Polym. Phys.*, 1977, **15**, 403.
- 13 N. Ramesh, P. Davis, J. Zielinski, R. Danner and J. Duda, *J. Polym. Sci. B-Polym. Phys.*, 2011, **49**, 1629.
- 14 M. Kanduč, W. K. Kim, R. Roa and J. Dzubiella, *ACS Nano*, <https://dx.doi.org/10.1021/acsnano.0c06319> (2020).
- 15 B. Amsden, *Macromolecules*, 1998, **31**, 8382.
- 16 L. Masaro and X. Zhu, *Prog. Polym. Sci.*, 1999, **24**, 731.

- 17 A. Gusev, F. Müller-Plathe, W. Van Gunsteren and U. Suter, Dynamics of small molecules in bulk polymers. In *Atomistic Modeling of Physical Properties*, Springer, 1994, pp 207.
- 18 J. Budzien, J. D. McCoy, D. Rottach and J. G. Curro, *Polymer*, 2004, **45**, 3923.
- 19 D. N. Theodorou, "Principles of molecular simulation of gas transport in polymers," in *Materials Science of Membranes for Gas Vapor Separation*, edited by Yu. Yampolskii, I. Pinnau and B. D. Freeman, Wiley, Hoboken, NJ, 2006, pp. 49-94.
- 20 L. Xi, M. Shah and B. L. Trout, *J. Phys. Chem. B*, 2013, **117**, 3634.
- 21 K. Zhang and S. K. Kumar, *ACS Macro Lett.*, 2017, **6**, 864.
- 22 D. Meng, K. Zhang and S. K. Kumar, *Soft matter*, 2018, **14**, 4226.
- 23 K. Zhang, D. Meng, F. Müller-Plathe and S. K. Kumar, *Soft matter*, 2018, **14**, 440.
- 24 T. Sentjabrskaja, E. Zaccarelli, C. De Michele, F. Sciortino, P. Tartaglia, T. Voigtmann, S. U. Egelhaaf and M. Laurati, *Nat. Commun.*, 2016, **7**, 11133.
- 25 M. Laurati, T. Sentjabrskaja, J. Ruiz-Franco, S. U. Egelhaaf and E. Zaccarelli, *Phys. Chem. Chem. Phys.*, 2018, **20**, 18630.
- 26 R. Higler, R. A. Frijns and J. Sprakel, *Langmuir*, 2019, **35**, 5793.
- 27 E. Lázaro-Lázaro, J. A. Perera-Burgos, P. Laermann, T. Sentjabrskaja, G. Pérez-Ángel, M. Laurati, S. U. Egelhaaf, M. Medina-Noyola, T. Voigtmann and R. Castañeda-Priego, *Phys. Rev. E*, 2019, **99**, 042603.
- 28 E. Martinez-Sotelo, M. Escobedo-Sánchez and M. Laurati, *J. Chem. Phys.*, 2019, **151**, 164504.
- 29 R. Poling-Skutvik, R. C. Roberts, A. H. Slim, S. Narayanan, R. Krishnamoorti, J. C. Palmer and J. C. Conrad, *J. Phys. Chem. Lett.*, 2019, **10**, 1784.
- 30 R. C. Roberts, R. Poling-Skutvik, J. C. Conrad and J. C. Palmer, *J. Chem. Phys.*, 2019, **151**, 194501.
- 31 W. Götze, *Complex dynamics of glass-forming liquids: A mode-coupling theory*, Oxford University Press, Oxford, UK, 2008.
- 32 R. Zhang and K. S. Schweizer, *J. Chem. Phys.*, 2017, **146**, 194906.
- 33 S. Mirigian and K. S. Schweizer, *J. Chem. Phys.*, 2014, **140**, 194506.
- 34 S. Mirigian and K. S. Schweizer, *J. Chem. Phys.*, 2014, **140**, 194507.
- 35 C. P. Flynn, *Point defects and diffusion*, Oxford University Press, Oxford, UK, 1972.
- 36 D. Emin, *Polarons*, Cambridge University Press, 2013.
- 37 K. S. Schweizer and E. J. Saltzman, *J. Chem. Phys.*, 2003, **119**, 1181.
- 38 K. S. Schweizer, *J. Chem. Phys.*, 2005, **123**, 244501.
- 39 E. J. Saltzman and K. S. Schweizer, *J. Chem. Phys.*, 2006, **125**, 044509.
- 40 E. J. Saltzman and K. S. Schweizer, *Phys. Rev. E*, 2008, **77**, 051504.
- 41 R. Zhang and K. S. Schweizer, *J. Chem. Phys.*, 2015, **143**, 144906.

- 42 R. Zhang and K. S. Schweizer, *J. Phys. Chem. B*, 2018, **122**, 3465.
- 43 J. Matthiesen, R. S. Smith and B. D. Kay, *J. Chem. Phys.*, 2010, **133**, 174505.
- 44 R. A. May, R. S. Smith and B. D. Kay, *J. Phys. Chem. A*, 2013, **117**, 11881.
- 45 J. N. Ryan and M. Elimelech, *Colloids Surf. A*, 1996, **107**, 1.
- 46 M. Kanduč, W. K. Kim, R. Roa and J. Dzubiella, *Macromolecules*, 2018, **51**, 4853.
- 47 J.-P. Hansen and I. R. McDonald, *Theory of simple liquids*, Elsevier, Amsterdam, 2006.
- 48 Y. Zhou, B. Mei and K. S. Schweizer, *Phys. Rev. E*, 2020, **101**, 042121.
- 49 Y. Zhou and K. S. Schweizer, *J. Chem. Phys.*, 2019, **150**, 214902.
- 50 B. Mei, Y. Zhou and K. S. Schweizer, *J. Phys. Chem. B*, 2020, **124**, 6121.
- 51 R. Verberg, I. De Schepper and E. Cohen, *Phys. Rev. E*, 1997, **55**, 3143.
- 52 E. Cohen, R. Verberg and I. De Schepper, *Physica. A*, 1998, **251**, 251.
- 53 E. J. Saltzman and K. S. Schweizer, *J. Chem. Phys.*, 2003, **119**, 1197.
- 54 J. C. Dyre, N. B. Olsen and T. Christensen, *Phys. Rev. B*, 1996, **53**, 2171.
- 55 J. C. Dyre, *J. Non-Cryst. Solids*, 1998, **235**, 142.
- 56 J. C. Dyre, *Rev. Mod. Phys.*, 2006, **78**, 953.
- 57 K. S. Schweizer and G. Yatsenko, *J. Chem. Phys.*, 2007, **127**, 164505.
- 58 H. A. Kramers, *Physica*, 1940, **7**, 284.
- 59 P. Hänggi, P. Talkner and M. Borkovec, *Rev. Mod. Phys.*, 1990, **62**, 251.
- 60 L. Verlet, *Mol. Phys.*, 1981, **42**, 1291.
- 61 M. Kinoshita, *J. Chem. Phys.*, 2003, **118**, 8969.
- 62 J. A. Perera-Burgos, J. M. Méndez-Alcaraz, G. Perez-Angel and R. Castaneda-Priego, *J. Chem. Phys.*, 2016, **145**, 104905.
- 63 B. Mei, Y. Lu, L. An and Z.-G. Wang, *Phys. Rev. E*, 2019, **100**, 052607.
- 64 S. Mirigian and K. S. Schweizer, *Macromolecules*, 2015, **48**, 1901.
- 65 R. Zhang and K. S. Schweizer, *Macromolecules*, 2016, **49**, 5727.
- 66 J. Yang and K. S. Schweizer, *J. Chem. Phys.*, 2011, **134**, 204908.
- 67 A. Ghosh, G. Chaudhary, J. G. Kang, P. V. Braun, R. H. Ewoldt and K. S. Schweizer, *Soft Matter*, 2019, **15**, 1038.
- 68 A. Ghosh and K. S. Schweizer, *J. Chem. Phys.*, 2019, **151**, 244502.
- 69 A. Ghosh and K. S. Schweizer, *Phys. Rev. E*, 2020, **101**, 060601.
- 70 G. Yatsenko and K. S. Schweizer, *Phys. Rev. E*, 2007, **76**, 041506.
- 71 M. Tripathy and K. S. Schweizer, *J. Chem. Phys.*, 2009, **130**, 244907.
- 72 A. Ghosh and K. S. Schweizer, *Macromolecules*, 2020, **53**, 4366.

- 73 Y. Zhou and K. S. Schweizer, *J. Chem. Phys.*, 2020, **153**, 114901.
- 74 Z. E. Dell and K. S. Schweizer, *Macromolecules*, 2014, **47**, 405.
- 75 A. D. Phan and K. S. Schweizer, *J. Chem. Phys.*, 2018, **148**, 054502.
- 76 V. Kobelev and K. S. Schweizer, *Phys. Rev. E*, 2005, **71**, 041405.
- 77 A. Ghosh and K. S. Schweizer, *J. Chem. Phys.*, 2020, **153**, 194502.